COMPARATIVE STUDY OF STRUCTURAL AND ELECTRO-OPTICAL PROPERTIES OF $CuInSe_2$ THIN FILMS IN THE COLD MICROPLASMA DEVICE

B.G. SALAMOV
Institute of Physics, Ministry of Science and Education,
AZ1073 Baku, Azerbaijan

The study investigates the impact of plasma-surface interaction on the structural, optical, and electrical properties of *$CuInSe_2$* (*CIS*) thin films. The films were characterized using various methods, including atomic force microscopy, X-ray diffraction, absorbance, transmission, and electrical measurements. The results show that plasma treatment significantly affects the electrical and optical properties of *CIS* films. The treatment increases transmission, decreases the absorption coefficient, and decreases band gap energy values from 1.05 to 0.88 eV. The resistivity values of *CIS* films at room temperature decrease by three orders of magnitude after plasma treatment. A planar cold microplasma device was used to visualize and record resistance inhomogeneity and photoconductivity distribution in a *$CuInSe_2$* copper-indium-diselenide film. The plasma-induced damage (*PID*) in a *$CuInSe_2$* film is primarily attributed to the efficacy of sputtering and physicochemical interactions within the discharge gap during the transition from Townsend to glow discharge. A nondestructive method was proposed for analyzing the kinetics of *PID* in the *$CuInSe_2$* film using fractal processing within the planar cold microplasma device. Fractal dimension analysis was employed to quantitatively assess the alterations in dynamic characteristics of the *PID* of *$CuInSe_2$* thin films. The film's quality was assessed through profile and spatially dispersed *DLE* intensity data, revealing surface inhomogeneity and degradation over time.

Keywords: $CuInSe_2$, X-ray diffraction, plasma-induced damage, thin film, discharge light emission, fractal dimension.
DOI: 10.70784/azip.1.2025356

1. Introduction

$CuInSe_2$ (*CIS*) is a ternary compound semiconductor exhibiting a chalcopyrite-type crystal structure upon solidification. It possesses a direct bandgap of approximately 1 eV, coupled with notable environmental stability under outdoor conditions. Owing to these advantageous characteristics, *CIS* is regarded as one of the most promising candidate materials for photovoltaic applications [1]. Cu–III–VI_2 compounds exhibit exceptionally high absorption coefficients, surpassing 10^5 cm^{-1} across the majority of the visible light spectrum. This absorption capability exceeds that of all other semiconductor materials currently employed in photovoltaic technologies. From the perspective of device optimization, the absorption coefficient is a key parameter influencing the selection of materials for the absorber layer in photovoltaic devices [2]. From the perspective of device optimization, the absorption coefficient is a key parameter influencing the selection of materials for the absorber layer in photovoltaic devices [3,4]. A central challenge in the deployment of *CIS* films in photovoltaic devices lies in the reproducible fabrication of films exhibiting optimal electrical and optical properties. The chemical interaction between oxygen and the photoactive layer material constitutes a primary mechanism underlying the degradation of optoelectronic devices and solar cells. Identifying correlations between interfacial properties and elemental characteristics provides insights into potential degradation pathways. Precise control over surface etching and oxidation processes is essential for the fabrication of devices with well-defined structural configurations [5].

Plasma etching of *CIS* film serves both to optimize the features of produced devices and to provide information about their thermal stability. The mechanism of surface oxidation during plasma etching of *CIS* thin films remains incompletely understood, and the experimental data obtained in air are inconsistent. Nonetheless, it is firmly known that these processes transpire and substantially affect the efficiency of solar cells. The annealing of *CIS* films in air diminishes surface resistance due to surface alignment and the repair of flaws. A previous study [6] demonstrated that the presence of oxygen affects various physical properties of *CIS* films, promoting the formation of an indium oxide (*In_2O_3*) phase, which in turn alters the systems' electrical and optical characteristics. Investigating the impact of *In_2O_3* on the optical properties and its formation on *CIS* films necessitates the application of more sensitive analytical techniques. However, while utilizing polycrystalline thin films rather than single crystals, it is imperative to exercise caution in regulating the system parameters, as the film is susceptible to damage [7]. The sensitivity of a device can be enhanced by decreasing the thickness of the semiconductor. This study experimentally reports the kinetics of plasma-induced damage (*PID*) in the *CIS* film, utilizing a direct current electric field at ambient temperature within a planar cold microplasma device (*CPD*). To quantitatively investigate the alterations in the dynamic characteristics of the *PID* of *CIS* thin films, we examined the film's quality by spatially distributed discharge light emission intensity (*DLEI*) data, which reveals surface inhomogeneity and degradation with time. Nonetheless, a significant deviation of its characteristics may be seen after prolonged operation in continuous mode. It is evidently associated with a modification in the surface characteristics of the semiconductor due to the prolonged influence of discharge plasma on the semiconductor electrode of the device [8].

131, H.Javid ave, AZ-1073, Baku
Institute of Physics
E-mail: jophphysics@gmail.com

As the importance of surface morphology increases, as seen in the above-mentioned studies, several techniques have been developed to characterise thin film surfaces, such as microscopic measurements including electron microscopy, atomic force spectroscopy, X-ray diffraction analysis and Auger electron spectroscopy [9,10]. However, these physical techniques cannot provide comprehensive information on a given thin film surface without a statistical approach. To obtain quantitative results that represent the entire surface of the thin film, the aforementioned techniques are often complemented by statistical or mathematical tools such as histograms, profiles, power spectral densities and fractal dimensions [9-12].

We can conclude that earlier analyses of the surface characterisation of thin films have mainly focused on identifying the surface properties, which are mostly generated by fabricating the film samples. Meanwhile, it is not possible to find a quantitative *PID* analysis of a thin film as a function of time using a fractal analysis process. In our previous studies, we proposed a non-destructive method involving fractal dimension analysis to measure the discharge light emission (*DLE*) homogeneity and resistivity of a GaAs semiconductor plate [13–15]. The present paper applies this method to time-dependent, spatially distributed *DLE* intensities in a thin film, providing an image of surface damage and determining the quality of $CuInSe_2$ over time.

Although *Cu*-rich films have superior structural features [16], their electrical characteristics are adversely affected by the existence of *Cu*-selenide secondary phases (e.g., Cu_2Se and $Cu_{2-x}Se$), which are deleterious to device applications [17,18]. In this context, it is evident that a comprehensive understanding of the material characteristics of these films is essential for the fabrication of high-efficiency solar cell devices [19].

This paper primarily examines the impact of non-thermal plasma treatment on the surface of thin films and its implications for the structural, optical, and electrical characteristics of CIS thin films in atmospheric air, to the best of our knowledge, for the first time. The majority of microstructural investigations of these polycrystalline materials are predominantly confined to SEM and XRD techniques. This study used AFM imaging and *DLE* to examine the structural properties of *CIS* films.

2. Experimental

Figure 1 illustrates the experimental configuration. In the planar cold plasma device, the *CIS* film was selected as the photocathode (5). The *CIS* film employed possesses a circular configuration with a diameter of 20 mm, situated on a glass substrate including a back contact. The soda-lime glass substrate was coated with a transparent conductor (*ITO*), followed by the deposition of a *CIS* (5) film approximately 250 nm thick using the triple-ionized beam technique (IBT), wherein *Cu*, *In*, and *Se* vapors for $CuInSe_2$ were ionized and accelerated [20]. During the deposition process, the acceleration voltages for the *Cu*, *In*, and *Se* beams were maintained at 2 kV, while the electron currents for their ionization were varied between 0 mA and 150 mA. The source materials utilized were *Cu*, *In*, and *Se* with a purity of 99.9999%. The source temperatures of the three crucibles for copper, indium, and selenium were 1420°C, 980°C, and 320°C, respectively. The substrate temperature was sustained at 300°C using an infrared lamp, while the vacuum chamber pressure was regulated to below 1×10^{-5} Torr for a deposition duration of 90 minutes. This plate is lit with infrared light (1), resulting in an enhancement of photoconductivity. A spectral filter (2) is utilized to selectively transmit the desired wavelength range to the cathode. The *CIS* film plays a critical role in image formation through its interaction with charged particle fluxes, including electrons and ions.

Positioned adjacent to the terminal side of the CIS layer is a glass substrate (9), coated with a transparent, conductive tin oxide (SnO_2) film (8). The SnO_2 layer exhibits a sheet resistance ranging from 15 to 20 Ω/sq. The SnO_2 and *ITO* electrodes are integrated into an external electrical circuit comprising a high-voltage DC source (U_0) and a series resistor (R_1), the latter serving as a current-sensing component. The application of a high potential difference (U_0) between the *ITO* electrode and the SnO_2 layer initiates an electrical discharge within the interstitial gap. The region confined between the *CIS* film and the glass plate constitutes the gaseous layer. An insulating mica sheet (7), featuring a central circular aperture, electrically isolates the inner surface of the *CIS* film from the planar anode. The adjustable thickness of the insulating layer enables modulation of the interelectrode gap, *d*, within the range of 15 to 40 μm. The standard diameter, *D*, of the electrode regions of the photocathode (or the gas discharge gap) is 9 mm. The experiments are conducted in air, and the measurements are taken at room temperature. Prior to the injection of gas into the system, the cell is evacuated to a pressure of 1×10^{-6} Torr. A voltage of up to 2.5 kV is delivered to the cell's electrodes. A uniform *GDLE* is observed over the entire electrode area with currents greater than 100 μA. The maximum E/N ratio is approximately 9 kTd. The GDLE is recorded using a *CCD* camera through a transparent anode.

The *DLE* from the cell is quantified using a computerized photon counting unit, specifically the photon counting head of a commercial Optically Stimulated Luminescence dating apparatus (*ELSEC 9010*). The unit's photomultiplier tube (*Thorn-EMI 9235 QA*) has exceptional sensitivity in the UV-visible range, aligning with the cell's emission. A glass filter that mostly transmits wavelengths between 330-700 nm (Schott BG39) is employed to eliminate IR leakage from the system. In addition to the time evolution of the DLE intensity, the temporal signal of the total current *I* through the *CPD* cell and the voltage drop *V* between the electrodes are

concurrently recorded.

The voltage-time and current-time curves recorded are digitised and transferred to a computer using an X-Y digitiser tablet. This unit also makes it possible to detect the dynamic behaviour of the discharge. Light intensity is then assessed by analysing the *DLE* (330–440 nm), which is recorded through a transparent anode. The apparatus has a dynamic range of at least 30. The minimum detected radiation energy density is $(6–8)\times10^{-4}$ J cm^{-2} in our setup. The *CIS* semiconductor film on the *ITO* film (4) side is uniformly illuminated by light from an incandescent lamp (75 W), which is transmitted through a Si filter ($\lambda \geq 0.9$ μm). When a negative potential is applied to electrode 4, the semiconductor *CIS* film in the gap (6) is bombarded by negative plasma elements (electrons and ions), which leads to plasma-induced damage to the surface of the *CIS* thin film and the formation of a damaged pattern on its surface. The *DLE* is registered by an intensified *CCD* camera. The homogenous image can then be processed or stored on a computer. This method ensures a spatial resolution of approximately 10 lp/mm.

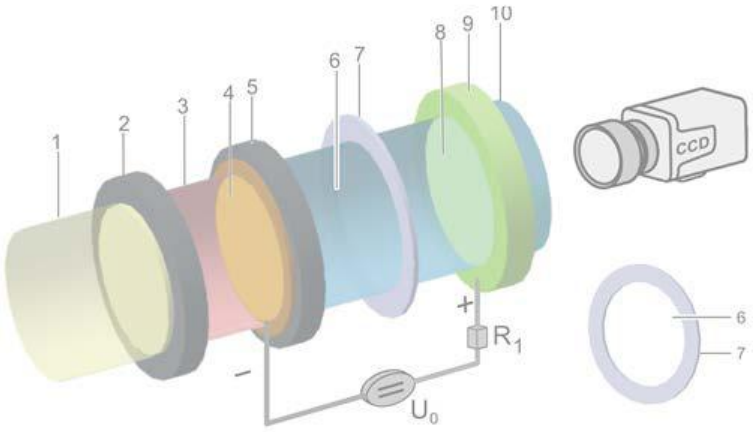

Fig. 1. Experimental setup. 1.light beam; 2. Si filter; 3. IR light beam; 4. semi-transparent *ITO* conductor; 5. *CIS* thin film; 6. gas discharge gap; 7. insulating mica foil; 8. semi-transparent SnO_2 conductor; 9. flat glass disc; 10. UV- visible light beam.

An optical absorbance spectrum was obtained using a UV+VIS spectrophotometer (*PerkinElmer Lambda 45*) in the wavelength range of 200–1100 nm. Light signals emitted by the samples were collected by an integrating sphere. The thickness of the composite films was measured using an infrared interference method based on the film's reflectance characteristics [21]. The resistivity of the $CuInSe_2$ films was measured using a two-point probe method with a Keithley 2400 source meter at room temperature. Surface morphology and grain size were studied using *AFM*.

3. Results and discussion

3.1. Structural characterization and morphological properties

Fig.2 illustrates the *XRD* pattern of a *CIS* film. The features of the 112, 220, and 116 diffraction lines of the chalcopyrite structure were observed. The three diffraction peaks with 2θ values of 26.78, 44.64, and 52.88 correspond to the (112), (220), and (116) reflections of chalcopyrite *CIS*, respectively. The *XRD* data unequivocally demonstrate that the as-deposited *CIS* films exhibit crystallization in the chalcopyrite structure. The pronounced (112) reflection compared to other peaks indicates that these *CIS* films possess a robust (112) texture, representing the close-packed plane of the chalcopyrite *CIS* structure [1]. The relative intensity indicates that the (112) axis is preferentially aligned perpendicular to the film surface. The surface morphology of the *CIS* film was analyzed using AFM to assess its surface roughness. Figure 3 illustrates the surface topography pictures captured for the *CIS* film prior to and subsequent to plasma treatment. In Fig. 3(a), clusters became evident alongside the crystalline structure in the untreated material. Clusters have vanished following plasma treatment as depicted in Fig.3(b). Nonetheless, the surface topography has formed clusters of disparate sizes with uneven configurations following plasma treatment (Fig. 3(b)). The surface morphology of the plasma-treated zone is evidently heterogeneous. The nonhomogeneous surface is additionally corroborated by resistivity measurements.

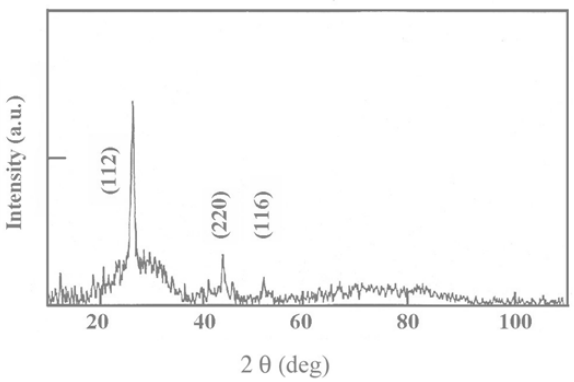

Fig.2. The X-ray diffraction pattern of *CIS* thin film.

Roughness can be related to the physico-chemical status of the surface under test. The roughness of *Cu*-rich films was found to exceed that of In-rich films. One of the factors contributing to this phenomenon has been identified as the presence of *Cu*-agglomerates in *Cu*-rich films [22]. The agglomeration process was verified through the utilisation of *AFM* analyses. Thus, roughness could include the physical limits of the solid surface in question, such as dust, contaminants and subsurface defects, all of which result in complex near-field structures of the diffracted field and the corresponding far-field propagated modes. In the micron or millimetre range, surface perturbations (scratches, grooves, grain relief, etc.) are spatially coherent, resulting from the preparation conditions. In [23], *Cu*-rich films had a surface with hills and valleys. In contrast, the topology of *In*-rich films was smoother. *AFM* studies revealed that the surface morphology of these In-rich films is dominated by a high density of relatively small, roughly circular clusters, with very little variation in height from cluster to cluster. This is in sharp contrast to the large, faceted grains present in *Cu*-rich films [19].

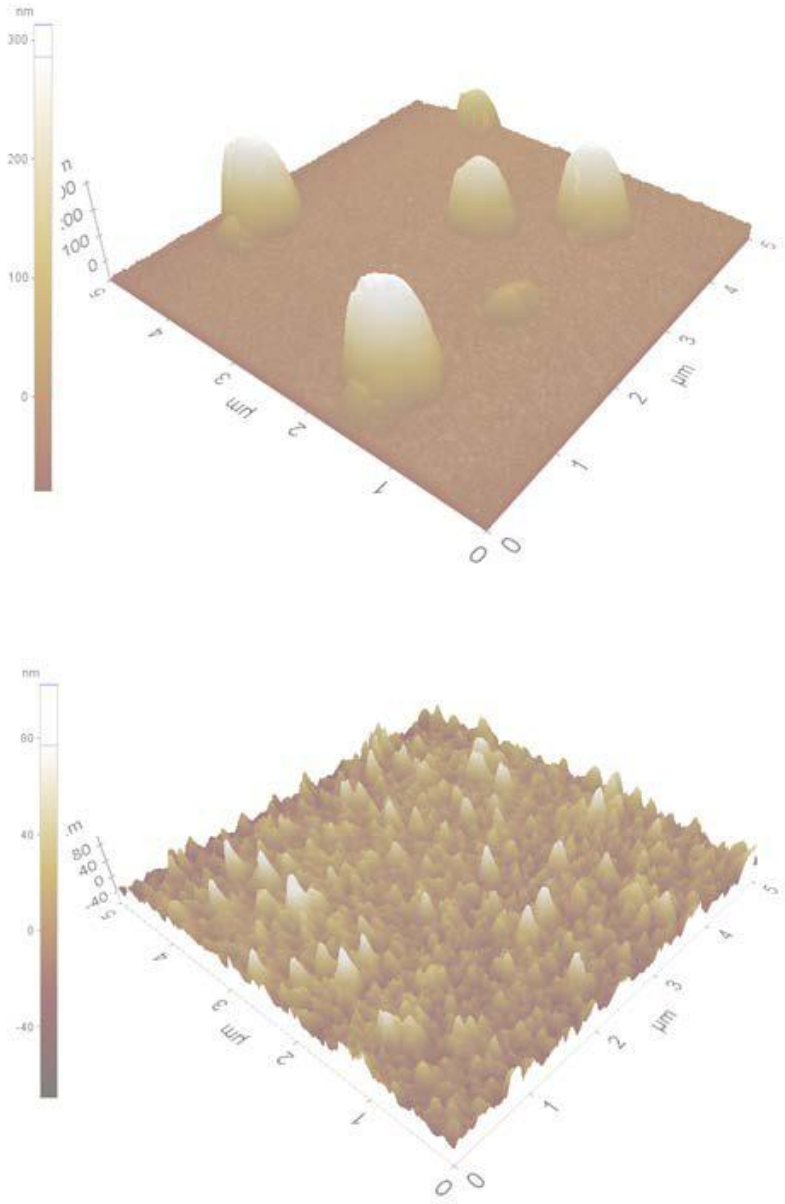

Fig.3. AFM images of the CIS film; a) before plasma treatment, b) after plasma treatment.

Figure 4 illustrates the typical variation in the number of photons emitted by the radiation over time when *CIS* is employed in the cold microplasma device (*CPD*). This may be due to the homogenisation of spatial conductivity, which affects the dynamic behaviour of the *DLE* in the gap. The figure also illustrates an excellent time response with a brief lag. However, the precise value of the lag could not be determined as it is shorter than the measuring system's time resolution. This short lag may be attributed to the reduction in beam-discharge lag caused by the dark current filling the traps. At the same time, the *DLE* increased rapidly in both darkness and under illumination, eventually saturating over time. However, the illuminated *DLE* is three times larger than the dark *DLE* at the beginning. The intensity of the

DLE around the electrode depends on the total resistance of the *ITO-CIS*-air gap-SnO_2 circuit. Therefore, it will be possible to adjust the intensity of the gas discharge glow by altering the resistivity of the *CIS* film. The resistivity of the *CIS* film can be adjusted by the *In/Cu* ratio up to values of 10^7 Ωcm [24], enabling its use as a semiconducting cathode in our system. The filamentation phenomenon can only be observed when the *CIS* film's resistance is less than a critical value for a given thickness.

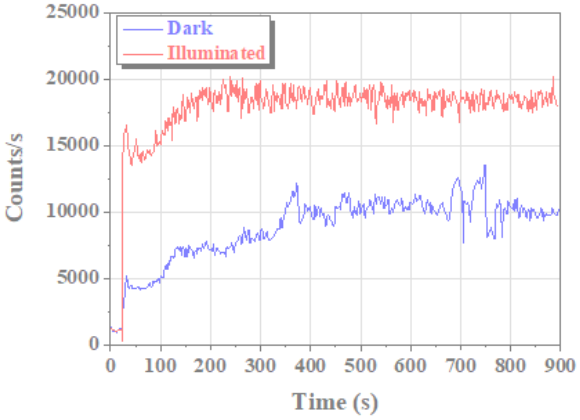

Fig.4. The dynamic behaviour of *DLE* intensity for $CuInSe_2$ sample. The system parameters are gap pressure p = 52 Torr, length of the discharge gap d =30 μm. The feeding voltage applied to the electrodes is 352 V.

However, Townsend discharges, in which a direct current flows at voltages close to the breakdown voltage (V_B), only occur in gases at low and moderate pressures for sufficiently low currents. The discharge usually becomes unstable as the current rises; either small regular oscillations or periodic, repetitive breakdown (relaxation oscillations) occur. This instability arises because the space charge produces a decreasing *CVC* of discharge [25]. The energy of the gas discharge charge particles and the sensitivity of this process depend on the high efficiency with which radiation intensity incident on the semiconducting plate is converted. Some of the discharge energy is transferred to the system's electrodes by bombardment due to electron-ion flow. This process leads to the sputtering of the electrode surface material [26]. It has been demonstrated that *PID* in a $CuInSe_2$ thin film is primarily due to the effectiveness of sputtering and physicochemical interactions in the discharge gap during the transition from the Townsend to glow discharge.

It was demonstrated that the *PID* in a *CIS* thin film was primarily the result of the effectiveness of sputtering and physicochemical interactions in the discharge gap during the transition from the Townsend to glow discharge. Surface profiler analysis was performed to characterise the surface state of CIS films after plasma treatment and establish changes in surface roughness. Following plasma treatment, the CIS films were represented as 3-dimensional (*3D*) charts showing the distribution of *DLEI* over time (see Fig.5). The visualisation possibilities have been evaluated; for example, a local change in surface inhomogeneity is determined by a local change in *DLEI*. A change in the *Cu/In* ratio in the studied films may result in the formation of *Cu* excess due to In vaporisation during the plasma process. This leads to the formation of Cu_2Se and *CuSe* excess on the surface of *CIS* and causes a change in discharge filamentation and surface inhomogeneity (see Fig. 5).

3.2. Analysis of the dynamics of plasma-induced damage in a $CuInSe_2$ thin film by fractal processing

Figure 5(a–e) presents the transformation of 2-dimensional (*2D*) surface patterns of *DLE* in the *CPD* with *CIS* film into *3D* surface patterns. The patterns were derived from the same *CIS* film with varying exposure durations (40, 50, 60, 70, and 90 seconds), resulting in distinct spatial resistivity distributions. As seen in Fig. 5, the dark regions are distributed against the light background. The dark areas indicate a low discharge current, resulting in high resistance of the *CIS* film. Accordingly, spatial variations in electrical resistance manifest as inhomogeneities in the *DLE* patterns [27]. If the non-uniformity in electrical conductance arises from plasma-induced structural degradation and variations in the indium-to-copper (*In/Cu*) ratio within the *CIS* film [24], then the spatial distribution of resistivity inhomogeneities can be effectively visualized. The comparison of the *DLE* pattern with the damaged surfaces enables us to conclude that the areas of structural disturbance correspond to regions of high resistivity inhomogeneities. An examination of the *DLE* pattern can ascertain the efficacy of visualizing conductance non-uniformities relative to their structure [28]. Consequently, the surface flaws observed in the *2D* image produced by the *DLE* can be understood as conductance non-uniformities situated inside a layer approximately equal to the thickness of the gas-filled gap. The measured *DLE* patterns of *CIS* film indicate that the regions of surface disturbance correspond to the buildup of inhomogeneities with high resistivity. In order to conduct a quantitative analysis of *DLE*s, it is essential to accurately identify and distinguish the bright and dark regions within the *2D* images of *CIS* films. As can be seen in Figures 5a–e, the *DLEI* is represented by a *3D* film surface pattern, which is used to highlight differences in intensity values between *2D* images. Fig. 5a differs from Fig. 5b–e in terms of its *DLEI* values, giving it an inhomogeneous spatial appearance due to plasma-induced damage in a $CuInSe_2$ thin film. However, Fig. 5b–e have heterogeneous surfaces due to much more variable *DLEI* distribution. Meanwhile, Figures 5a–e, which show the transformation of the *DLEI* into profile form in the active *CIS* film area in pixels, clarify the differences between the *3D* patterns more efficiently over time.

Changes to the central surface of the film are clearly visible (see the 40 s profile in Fig.5), with high *DLEI*. The lateral regions have higher resistivity values; therefore, the *DLEI* is lower compared to the central region of the film. Interestingly, the entire surface of the thin film can be easily identified by the

spatial pattern. In our case, the differences in *DLEI* values between pixels on the diameter of the thin film are 241, 119, 98, 147 and 183 (see Fig. 5 and Table 1). Note that profiles can only provide limited values for *DLEI*, as any profile can be measured along a specific diameter of the *DLE* pattern. However, it is clear from the profiles that damage initially starts in the central regions of the film due to a high intensity difference (i.e. 241). Over time, the difference between the maximum and minimum intensities decreases to around 60 s (see Table 1). Then, the difference increases again at 70 and 90 seconds. Considering the exposure time range of 40–70 seconds, the central regions of the film were damaged first due to lower resistivity. Later on, the lateral regions of the film were damaged since the current, and consequently the *DLEI*, is higher in the lateral regions, as can be seen at 60 s, 70 s and 90 s. The intensity value cannot exceed a certain value at the centre of the film (see the pattern at 90 s). In conclusion, the above-mentioned process shows that spatial damage to the film occurs quite quickly in our cold plasma device, meaning that the film is almost entirely damaged after 100 seconds.

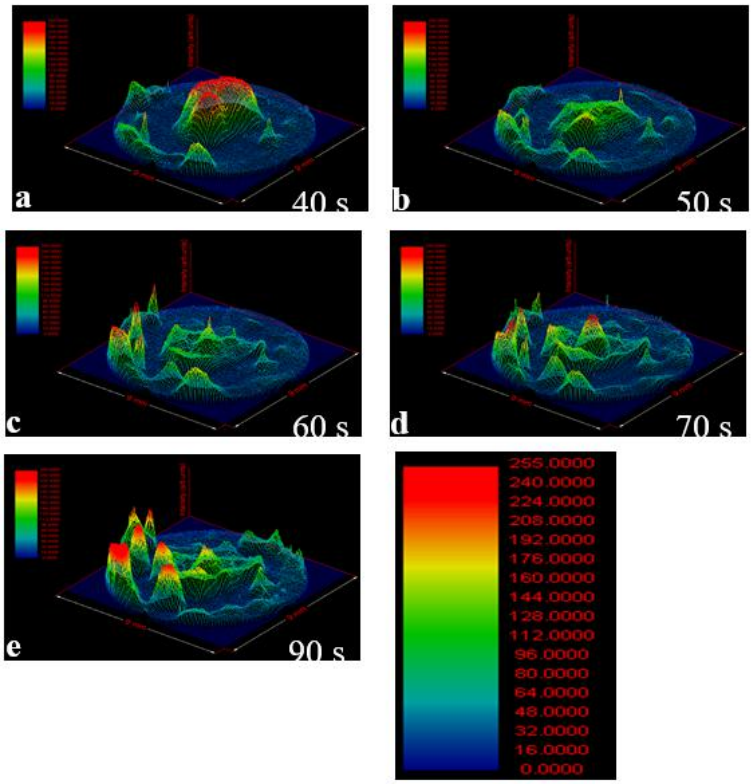

Fig. 5 The *3D* surface patterns of a $CuInSe_2$ films in the cell in gray level scales.

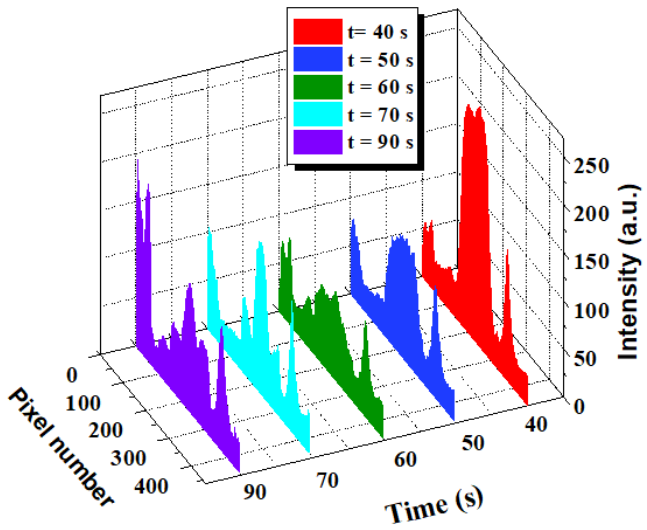

Fig. 6. Variations of *DLE* intensity profiles (i.e. gray levels) crossing the active area of *3D* surface pattern of *$CuInSe_2$* film with respect to time.

The next step is to estimate the fractal dimension in order to identify the damaging effects in the spatial patterns shown in Fig. 5a-e, over the active area of *DLEI*. Damage to the film is caused by bombardment of the electrode surface due to an electron-ion flow within our voltage range. Therefore, the greater the damage to the film, the higher the fractal dimension values. Under optimum conditions, it is possible to calculate *3D* representations of thin film surfaces. In order to use similar terminology for the *DLE* pattern and the analysis process, we should note that *DLEI* values are referred to as 'gray levels', and the term 'grid' is used for 'pixel'. In this manner, fractal dimension analysis was realised by calculating *L(R)* for various *R* values within a 960 x 960 pixel area with a maximum of 256 grey levels for each pattern. Figures 7a–e show the results of the analysis in the form of log-log plots of each pattern with least squares linear fit lines for different times.

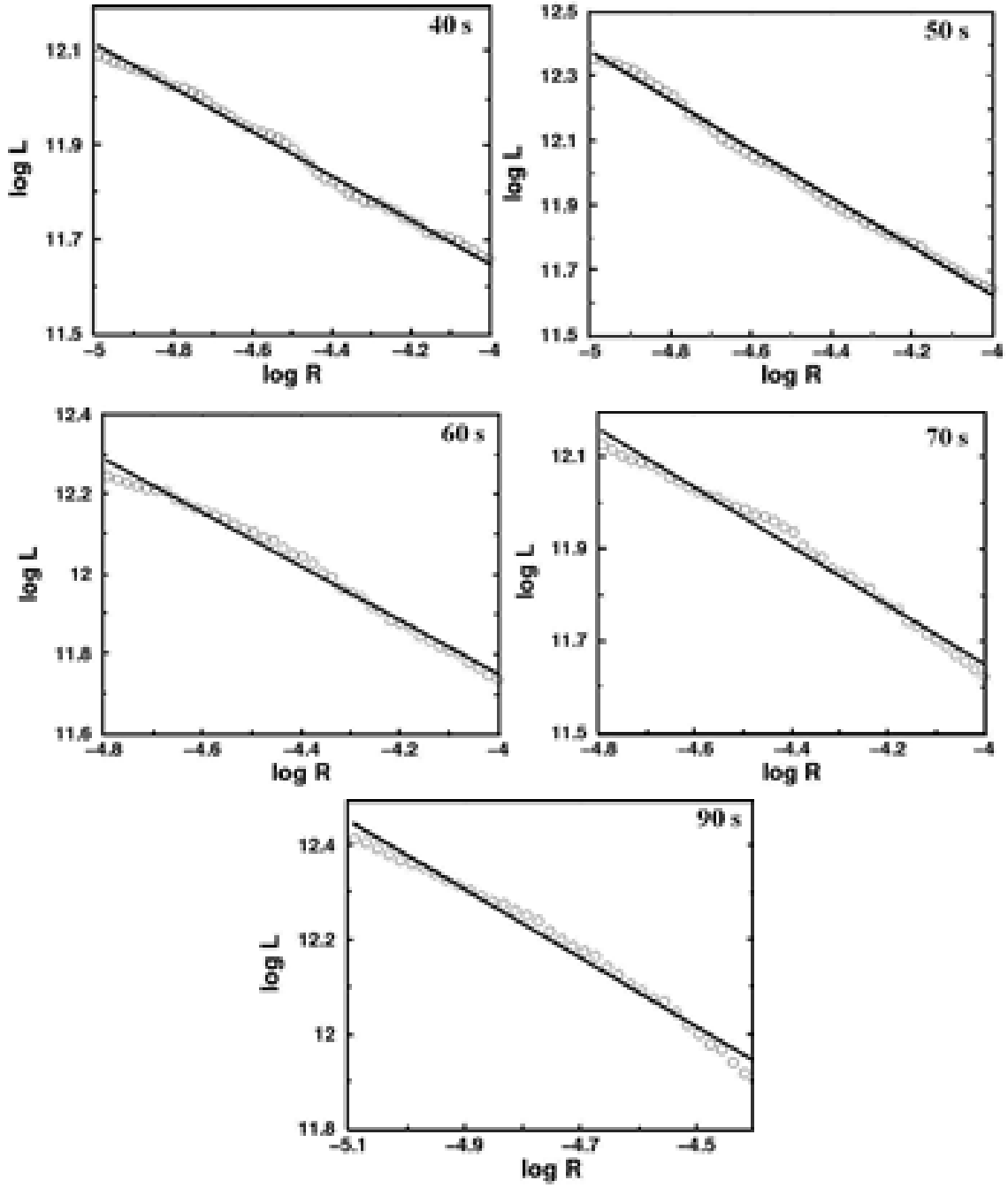

Fig.7. The log-log plots of the *DLE* intensities for surface patterns in Fig.5a-e.The plots are by increasing time.

The dimension values were extracted from the slopes of the linear fit lines. As can be seen in Table 1, the dimension values change according to the slopes in these plots. These values provide insight into the damaging process of the active area of the *DLE* surface pattern on the film, in that high values indicate excess filled grids relating to the grey levels.

Table 1.
The results of analyses for five patterns of *DLE* distribution at different times.

Spatial pattern	Analyses	Profile	Fractal Dimension
(a) 40 s		241	2.462 ±0.004
(b) 50 s		119	2.751 ±0.006
(c) 60 s		98	2.673 ±0.011
(d) 70 s		147	2.633 ±0.011
(e) 90 s		183	2.721 ±0.014

The initial dimension value of the DLE pattern seen in Figure 5a is determined to be 2.462, noting that the maximum value of *D* is 3. This results in an inhomogeneous look owing to its low *D* value, so the damage to the film surface is limited. Furthermore, the *DLE* amplifies in the central part of the film. The initial evident damage manifests at the center of the film. With the increase in time, the dimension values exhibit variability (refer to Table 1). At 50 seconds, the dimension attains its maximum value of 2.751, signifying the peak variability in *DLE* intensity over time. At this exposure duration, the deterioration to the film reaches its peak. At 60 seconds and 70 seconds, the dimension exhibits a declining trend, measuring 2.673 and 2.633, respectively. Nonetheless, this declining trend is supplanted by an ascending trend at 90 seconds (refer to Table 1). Additionally, the discrepancies between maximal and minimal DLE intensity values in Table 1 (profile column) generally suggest an association with the dimension values, with the exception of the 60 s and 90 s cases. Generally, greater discrepancies between peak and minimal DLE intensity levels correspond to lower fractal dimension values. The exceptions arise because the dimension values are computed throughout the whole surface of the thin film, encompassing all *DLE* intensities per pixel, whereas the profile values provide only a superficial assessment of the filled grids along a diameter.

We have taken over 30 *DLE* patterns from different samples and system parameters. Figure 5 shows five of these *DLE* patterns for the same sample. The results can be summarised as follows: The main conclusion that can be drawn from the surface patterns is that the *DLE* intensity varies spatially. This suggests that the *PID* of *CIS* (and similar) films can be visualised using our system. However, the *DLE* is not stable enough to produce a well-focused pattern, as in the case of *GaAs*, which may be due to the instability of the electrical (and possibly optical) properties of *CIS* samples when ionisation system parameters, such as space charge and temperature, change over time. The results showed that the surface pattern of a thin film changes when the *CIS* sample is illuminated. However, as mentioned above, the *DLE* intensity is highly unstable, making the pattern sensitive to different discharge parameters (e.g. feeding voltage, pressure and discharge gap).

3.3. Optical properties

Figure 8 shows the transmission spectra of *CIS* films in the wavelength range of 200–1000 nm, both before and after plasma treatment. We hypothesise that In segregated from the surface of the *CIS* samples during plasma treatment, consequently increasing the *Cu/In* ratio. As the *Cu/In* ratio increases, so does the transmission. The experimental results show that plasma etching of the *CIS* layers has the same effect as annealing in air. This positive influence of plasma etching on *CIS* film parameters can be attributed to the adsorption and desorption of oxygen from the grain particles at the surface borders. Nevertheless, the absorbance of all samples is high in the visible region. Additionally, the observed increase in optical transmittance in *Cu*-rich samples may be due to the presence of $Cu_{2-x}Se$ ([29]).

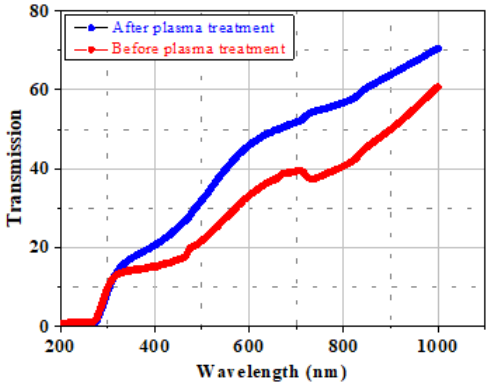

Fig. 8. The optical transmission of *CIS* thin films as a function of plasma treatment.

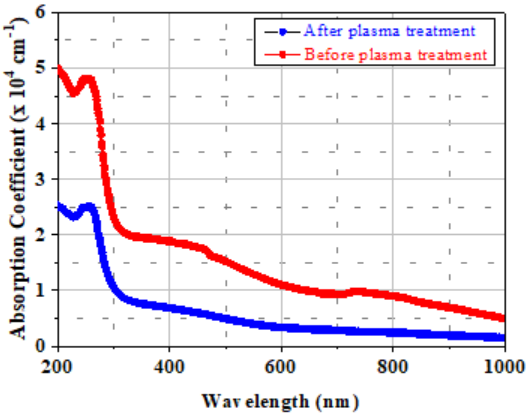

Fig. 9. The optical absorption coefficient of *CIS* thin films as a function of plasma treatment.

Figure 9 shows how the absorption coefficient (α) varies with wavelength. Before plasma treatment, it is clear that the absorption coefficient increased up to a value of $2x10^5$ cm^{-1}. Conversely, after plasma treatment, the absorption coefficient decreased considerably. An earlier spectroscopic investigation [30] established that changes in the absorption coefficient value in *CIS* films and crystals are not connected with oxide formation. This is because if the oxide layer from the sample's surface is released by plasma etching immediately prior to measuring the

absorption, the absorption coefficient value also increases. Studies of such films reveal a significant selenium concentration gradient near the surface. Accordingly, changes in the absorption coefficient are associated with significant variations in the composition of the film layers.

The electronic transition between the valence and conduction bands can be direct or indirect. In the former case, electron transitions are permitted if the transition probability p is greater than zero; in the latter case, they are forbidden. The transition probability is given by (1)

$$(\alpha h\nu)^p = A(h\nu - E_g) \quad (1)$$

where E_g denotes the band gap, $h\nu$ the energy of the incident photon and A is a constant. The exponent p is a number which characterizes the transition process and value of p = 1/2, 2/3 or 2 for indirect allowed, direct forbidden or direct allowed transitions, respectively.

The nature of transition in the film can be determined by plotting $(\alpha h\nu)^p$ against photon energy $h\nu$ for suitable value of p which yields straight line behavior. The band gap E_g is determined by plotting $(\alpha h\nu)^p$ against photon energy $h\nu$ for suitable value of p the graph is a straight line and the value of E_g is obtained by extrapolating the linear portion of the graph to intercept the photon energy axis [31]. The optical band gap E_g can be obtained from the graph of $(\alpha h\nu)^2$ versus $h\nu$, which is illustrated in figure 10. With the treatment of plasma, the band gap energy value decreases from 1.04 to 0.88 eV. This situation is strongly related to the *Cu/In* ratio [29,32].

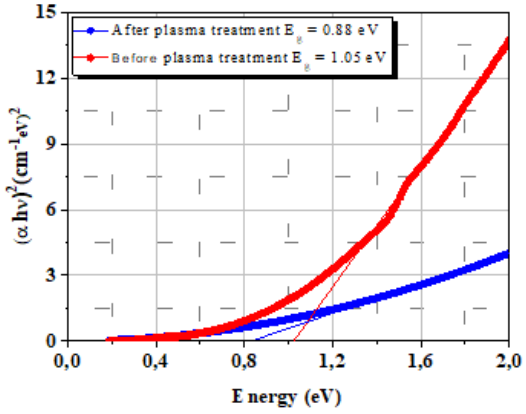

Fig. 10. The $(\alpha h\nu)^2$ versus $h\nu$ curves of *CIS* thin film before and after plasma treatment.

3.4. Electrical properties

The resistivity (ρ) of $CuInSe_2$ films was measured at room temperature using the two-point probe method, both before and after plasma treatment. It is clear that the ρ values of regions exposed to plasma treatment are not homogeneous. The variation in ρ of the *CIS* film is given numerically in Table 1. Current filamentation (high current density) has primarily started clusters, as can be seen in the *AFM* images in Figure 3(a). We hypothesise that In segregated from the surface of the *CIS* samples during plasma treatment, consequently increasing the *Cu/In* ratio. ρ is strongly related to the *Cu/In* ratio. An increase in the *Cu/In* ratio causes a decrease in the ρ of the sample. As can be seen in Table 1, the ρ values decrease by three orders of magnitude after plasma treatment. This result is consistent with ρ variations reported previously [1]. In [29], the Cu/In ratio increased from 0.9 to 1.1, resulting in a five-order-of-magnitude decrease in resistivity. An increase in ρ occurs when the copper concentration decreases relative to the indium concentration, due to the excess In atoms acting as donors. The drastic decrease in ρ observed could be attributed to the high conductivity of the $Cu_{2-x}Se$ phase segregated at the grain boundaries [29]. Additionally, copper excess causes a degeneracy in the deposited films. However, this result clarifies the decrease in the optical band gap. It should be noted that the electric characteristics of *CIS* layers are determined by the interaction between oxygen and natural defects, and the width of the band gap depends on the perfection of the crystal structure of the thin film [33].

Table 1.
The resistivity of *CIS* films before and after plasma treatment.

CIS Resistivity (Ωcm)	
Before plasma treatment	After plasma treatment
1.7×10^7	1.0×10^4
	8.5×10^4
	3.5×10^5
	1.1×10^6
	1.2×10^6
	3.3×10^6

4. Conclusion

The gas discharge stabilisation phenomenon by a high-resistivity photocathode is applicable to all semiconducting films with a resistivity between 10^6 and 10^9 Ω·cm. $CuInSe_2$ and similar films can be used with our cold microplasma device to adjust the sensitivity range. PIDs in thin films are important for obtaining optimal system running conditions and enabling ideal thin film manufacturing processes. We performed a quantitative analysis to identify the time-dependent damaging effects on a $CuInSe_2$ thin film. We demonstrated that the *PID* in a $CuInSe_2$ thin film was primarily due to the effectiveness of sputtering and physicochemical interactions in the discharge gap during the transition from the Townsend to glow discharge. At the same time, *PID* is a fast process that affects the electrical and optical properties of our cold microplasma device. Increasing exposure time results in a change in the location of the damaged areas over the surface, and fractal analysis of the entire surface of the thin film can be used to determine the order of damage. Thus, the most appropriate physical parameters for thin films can be selected by applying fractal analysis. The damaging effect of space charge

on a thin film surface can be reduced by using inert gases such as xenon and by operating the device in pulses. In all cases, fractal dimension calculations determine the extent of the damaged area on the thin film. Additionally, this analysis is performed on the entire active area of the *CIS* film, and the *DLE* intensity values among pixels on the surface pattern's diameter may not provide an accurate result for the entire spatial pattern.

We investigated the effect of plasma-surface interactions on the structural, optical, and electrical properties of *CIS* thin films. *XRD* analysis revealed that the films exhibit a chalcopyrite phase and a preferential (112) orientation. We found that plasma treatment plays an important role in the electrical and optical properties of *CIS* films. Following plasma treatment, transmission increases while the absorption coefficient decreases. The band gap energy value decreases from 1.04 to 0.88 eV with plasma treatment. The resistivity values in regions exposed to plasma treatment are not spatially homogeneous and decrease by three orders of magnitude following treatment. The resistivity of the *CIS* thin film is strongly related to the *Cu/In* ratio. A change in the *Cu/In* ratio in the studied films may result in the formation of *Cu* excess due to In vaporisation during the plasma process. This results in the formation of Cu_2Se and *CuSe* excess on the surface of *CIS* and leads to changes in discharge filamentation and surface inhomogeneity. Increasing the optical transmittance and decreasing the resistivity are both required for improved performance of *CIS* thin films. The results of the investigation (i.e. the interactions of oxygen with the surface of the *CIS* films and the methods of oxidising this three-component semiconductor material) show that this type of plasma etching has a positive influence on the parameters of devices based on it.

ACKNOWLEDGEMENTS

The author would like to thank Prof. Dr. K. Sato and Mr. K. Tanaka from the Faculty of Technology, Tokyo University of Agriculture and Technology, for supplying CIS samples.

[1] *Z.Z. Yan Zhang, Y. Liu, H. Gao, Y. Mao*, Mater. Sci. Semiconduct. Process. 120, 105267, 2020.

[2] *Z.Z. Yan Zhang, Y. Liu, H. Gao, Y. Mao*. Organ. Electron. 67, 168–174, 2019.

[3] *S.K.B. Joo Sung Kim, et al.* Nano Energy 18, 30033–30038, 2018.

[4] *T. Meyer, F. Engelhardt, J. Parisi and U. Rau*. J. Appl. Phys. 91, 5093, 2002.

[5] *I. H. Raja Azadar Hussain*, Solid State Sci. 100, 106101, 2020.

[6] *J. Müller, J. Nowoczin, H. Schmitt*, Thin Solid Films 496(2):364-370 DOI:10.1016/j.tsf.2005.09.077 , 2006.

[7] *H.Y. Kurt, E. Kurt and B.G. Salamov*, Cryst. Res. Technol. 41, 698, 2006.

[8] *E.L. Gurevich, S. Kittel, R. Hergenröder, Y.A. Astrov, L.M. Portsel, A.N. Lodygin, V.A. Tolmachev and A.V. Ankudinov*. J. Phys. D: Appl. Phys. 43, 275302, 2010.

[9] *K.S. Urmila, T.A. Namitha, B. Pradeep*. Intern. J. Recent Research and Review (IJCRR) VIII(4), 6, 2015.

[10] *Y. Wang and K. W. Xu.* Thin Solid Films 468, 310-315, 2004.

[11] *Z. W. Chen, X. P. Wang, S. Tan, S. Y. Zhang, and J. G. Hou*. Physical Review B. 63, 165413 2001.

[12] *K. Malek*, Thin Solid Films 408, 73-78, 2002.

[13] *H. Y. Kurt, E. Kurt, and B. G. Salamov*, The Imaging Sci. J. 49, 205-212, 2001.

[14] *B. G. Salamov, H. Y. Kurt, and E. Kurt*, The Imaging Sci. J. 51, 187-197, 2003.

[15] *H. Y. Kurt, E. Kurt, and B. G. Salamov*, Cryst. Res. and Tech. 39 (9): 743-753, 2004.

[16] *L. Gutay, D. Regesch, J.K. Larsen, Y. Aida, V. Depredurand, S. Siebentritt*, Appl. Phys. Lett. 99, 151912, 2011.

[17] *H.S. Min, S. Mandati, R. Chandran, A. Mallik, M. Arif, S. Bhuiyan, K.G. Deepa*, Orient. J. Chem., 2019, 35, 01-13.

[18] *M. Kemell, M. Rital, M. Leskel*, Solid State and Mater. Sci., 2005, 30, 1–31, doi: 10.1080/10408430590918341.

[19] *T. Feurer, R. Carron, G.T. Sevilla, F. Fu, S. Pisoni, Y.E. Romanyuk, S. Buecheler and A.N. Tiwari*. Adv. Energy Mater. 2019, 9, 1901428, doi: 10.1002/aenm.201901428

[20] *K. Tanaka, M. Kosugi, F. Ando, T. Ushiki, H. Usui and K. Sato*, Jpn. J. Appl. Phys. 32, 113, 1993.

[21] *S.M.F. Hasan, M.A. Subhan and K.M. Mannan*, Opt. Mater. 14, 329, 2000.

[22] *R. Jayakrishnan, T. Sebastian, T.T. John, C.S. Kartha and K.P. Vijayakumar*, J. Appl. Phys. 102, 043109, 2007.

[23] *R. Jayakrishnan, P.M. Ratheesh Kumar, C.S. Kartha and K.P. Vijayakumar*, Meas. Sci. Technol. 17, 3301, 2006.

[24] *J.-M. Cho*, Journal of Nanoelectronics and Optoelectronics, 5, N 2, 218-221, 2010.

[25] *B. G. Salamov and H. Yucel Kurt*, J. Phys. D: Appl. Phys. 38 (5), 682-687, 2005.

[26] *B. G. Salamov, A. Gunen.*, Imaging Sci. J. 49 (N 2), 101-111, 2001.

[27] *L. V. Belyakov, A. Mageramov and L. G. Paritskii*, Sov. Phys. Semicond. 12, 739, 1978.

[28] *B. G. Salamov, K. Colakoglu and S. Altindal*, Infrared Phys. & Technol. 36, 661, 1995.

[29] *A.A. Akl and H.H. Afify*, Mater. Res. Bull. 43, 1539, 2008.

[30] *M.R. Balboul, A. Jasenek, O. Chernykh, U. Rau and H.W. Schock*, Thin Solid Films 387, 74, 2001.

[31] *S. Agilan, D. Mangalaraj, S.K. Narayandass and G. Mohan Rao*, Physica B 365, 93, 2005.

[32] *R.R. Philip, B. Pradeep, G.S. Okram and V. Ganesan*, Semicond. Sci. Technol. 19, 798, 2004.

[33] *L. Kronik, U. Rau, J.F. Guillemoles, D. Braunger, H.W. Schock and D. Cahen*, Thin Solid Films 361, 353, 2000.

Received:12.09.2025